



Surface reconstruction engineering of twinned Pd₂CoAg nanocrystals by atomic vacancy inducement for hydrogen evolution and oxygen reduction reactions



Suli Liu^{a,b,*}, Hui Zhang^a, Xueqin Mu^{a,b}, Changyun Chen^a

^a Key Laboratory of Advanced Functional Materials of Nanjing, Nanjing Xiaozhuang University, Nanjing 211171, China

^b Jiangsu Collaborative Innovation Center of Biomedical Functional Materials and Jiangsu Key Laboratory of Biofunctional Materials, School of Chemistry and Materials Science, Nanjing Normal University, Nanjing, 210023, PR China

ARTICLE INFO

Keywords:

Twinned Pd₂CoAg nanocrystal
Atomic vacancy
Electrocatalyst
HER
ORR

ABSTRACT

The integration of different active sites into metallic catalysts, which may impart new properties and functionalities, is desirable yet challenging. Herein, a novel strategy is demonstrated to integrate atomic vacancies onto a twinned Pd₂CoAg surface. This strategy shows that such integration is highly efficient for hydrogen evolution reaction (HER) and oxygen reduction reaction (ORR) catalysis at room temperature. We characterize the composition and structure of the twinned Pd₂CoAg nanocrystals with vacancy (v-Pd₂CoAg NCs) interfaces and it is shown that the Co addition not only increases the atomic vacancies of Pd₂Ag twinned interface, but also leads to the formation of oxygen vacancies on the surface of CoO_x. The synergistic effect of the surface atomic vacancies and metal twinned interfaces of v-Pd₂CoAg NCs can tune the charge-density distribution on the surface of the electrocatalysts, and result in a 5 times increase in ORR mass activity than that of Pt/C at 0.9 V. This study provides a foundation for the rational design of ‘active sites’ for practical HER and ORR electrocatalysts.

1. Introduction

Controlling the exterior surface structure of the electrode materials can be used to enhance the activity of catalysts, which has been widely applied for the sustainable conversion processes of water-hydrogen-oxygen including the oxygen reduction reaction (ORR) and hydrogen evolution reaction (HER) [1–5]. Generally, Pt-based catalysts exhibit good stability, low Gibbs free energy, and superior electrocatalytic performances, but their high cost and low abundance pose a serious limitation for global-scale applications [6–9]. Thus, the prompt development demands advanced efficient multifunctional electrocatalysts toward HER and ORR with low cost as well as high electrocatalytic activities [10–12]. Recently, the development of palladium (Pd)-based nanocrystals (NCs) provides a promising strategy because Pd is less costly and more abundant than Pt, which exhibits a great potential in catalyzing the HER and ORR. However, their electrocatalytic activity and durability are inferior to Pt [13,14]. To overcome the above limitations, the active site-rich core-shell nanostructure has been demonstrated as a promising alternative [15,16]. Such an interface structure can maximize the utilization efficiency of active metals by tuning their composition, thereby displaying a high electrocatalytic activity with

low amount of noble metals. [17,18]. To reach an ideal equilibrium state, making a rational design of Pd-based NCs with precise surface tuning is highly desirable but remains a formidable challenge.

Determining the chemical structure of active sites is a key step in understanding how a heterogeneous catalyst works [17–23]. As reported, the surface defect engineering (such as step edges, stacking faults, vacancies, lattice-strained sites, and surfaces of amorphous materials) of electrocatalysts can tune the electronic properties of catalysts to increase the chemical adsorption and active sites, and thus improves the catalytic activity [17–19]. Meanwhile, multicomponent active sites have provoked fast-growing interest for manufacturing efficient metal catalysts [20,18–23]. Thus, to facilitate the activation of reagents, the surface reconstruction of metal nanocrystals with intrinsic defects (vacancies) have emerged as an effective method to prepare heterogeneous catalysts with improved activities, especially in some tandem reactions. Very recently, Zuo and co-workers found that the PdCuCo catalyst with abundant vacancies played a vital role in affecting the ORR and oxidation of alcohols with excellent activity [17]. Thus, the noble metal catalysts with controllable defects have great potentials for enhancing their electrocatalytic performance.

Herein, we report on a simple, one-pot, solid-liquid phase method

* Corresponding authors at: Key Laboratory of Advanced Functional Materials of Nanjing, Nanjing Xiaozhuang University, Nanjing 211171, China.

E-mail addresses: niuniu_410@126.com (S. Liu), cychen@njzxc.edu.cn (C. Chen).

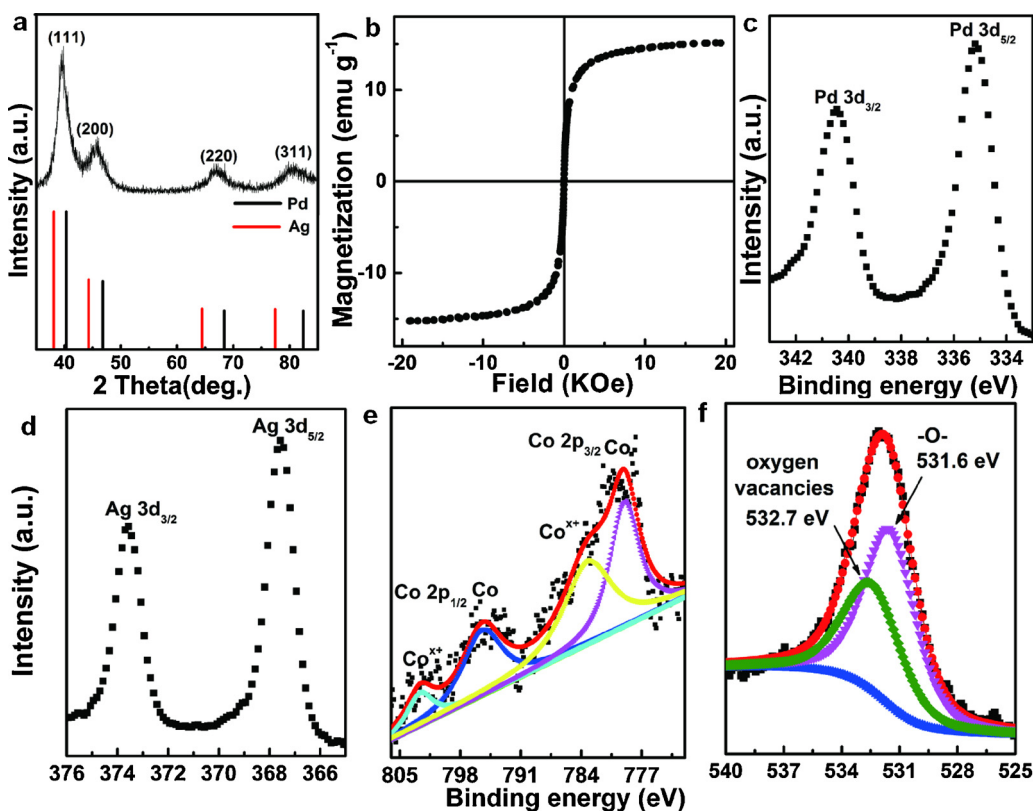


Fig. 1. (a) XRD pattern and (b) Field-sweep of the magnetization at 300 K of v-Pd₂CoAg NCs. XPS spectra of the (c) Pd 3d, (d) Ag 3d, (e) Co 2p, and (f) O 1 s regions for the sample.

for fabricating Pd₂CoAg NCs with abundant vacancies (v-Pd₂CoAg) as the starting materials to achieve a high catalytic performance towards the HER and ORR. The detailed electrochemical studies expose that the v-Pd₂CoAg electrocatalyst possesses a remarkable electrocatalytic activity for HER in acidic solutions with a smaller overpotential at -10 mA cm⁻² (24 mV) and a lower Tafel slope (28 mV dec⁻¹), as well as long term stability. In addition, its ORR activity is similar to those of Pt catalysts in acidic solutions. These suggest that the twinned interface and the surface with abundant vacancies can tune the binding of H or O atoms, resulting in a 5-fold increase in ORR mass activity compared with that of Pt/C at 0.9 V.

2. Experimental section

2.1. Synthesis of v-Pd₂CoAg NCs

In a typical synthesis, Pd(NO₃)₂ (~ 1 mmol) and Co (acac)₂ (~ 0.5 mmol) were added in the 10 mL of 1-octadecene (ODE). Then, 6 mL of oleylamine (OLA) was introduced, and the reactor was heated to 250 °C for 5 min. Subsequently, the AgNO₃ solution was rapidly injected into the mixture and maintained for 25 min. After the addition was completed, the black product was collected by centrifugation. Finally, the precipitate was dried in an oven at 40 °C. The metal content of the Pd₂CoAg was controlled by the molar ratios of metal precursors (Pd-Co-Ag = 2-1-1).

2.2. Synthesis of Pd₂Ag NCs

Pd₂Ag NCs were also synthesized using the method similar to that for v-Pd₂CoAg. In this case, only Pd(NO₃)₂ and AgNO₃ were employed as the metal precursors [24].

2.3. Synthesis of G/v-Pd₂CoAg NCs [24]

20 mL of v-Pd₂CoAg NCs dispersion (2 mg/mL) was added into 20 mL of DMF solution of graphene (0.5 mg/mL), then the mixture was sonicated for 140 min to obtain samples.

2.4. Electrochemical measurements

ORR measurements were performed with an Autolab PGSTAT302 N system in N₂ or O₂-saturated 0.1 M KOH solutions. In all measurements, the Ag/AgCl reference electrode was calibrated with respect to the reversible hydrogen electrode (RHE), and the counter electrode used was a platinum foil. Meanwhile, HER measurements were also performed with a CHI, 660E workstation in the 0.5 M H₂SO₄ and 1.0 M KOH solutions. In all measurements, the counter electrode used was a graphite rod. The overall catalyst loading was 0.283 mg cm⁻².

2.5. Structural characterization

X-ray diffraction tests (XRD) tests were carried out on a D/max 2500 VL/PC diffractometer (Japan) with Cu K α radiation ($\lambda = 1.54060 \text{ \AA}$). The transmission electron microscopy (TEM) and high-resolution transmission electron microscopy (HRTEM) images were obtained on JEOL-2100 F apparatus, which is equipped with scanning transmission electron microscopy (STEM) and EDS detectors that can be used for elemental mapping analysis. The atomic structure of the v-Pd₂CoAg NCs was characterized using an ARM-200CF (JEOL, Tokyo, Japan) transmission electron microscope operated at 200 keV and equipped with double spherical aberration (Cs) correctors. The attainable resolution of the probe defined by the objective pre-field was 78 pm. Magnetic measurements were performed on a superconducting quantum interference device (SQUID) magnetometer (MPMS XL-VII SQUID). The X-ray photoelectron spectra (XPS) were recorded on a

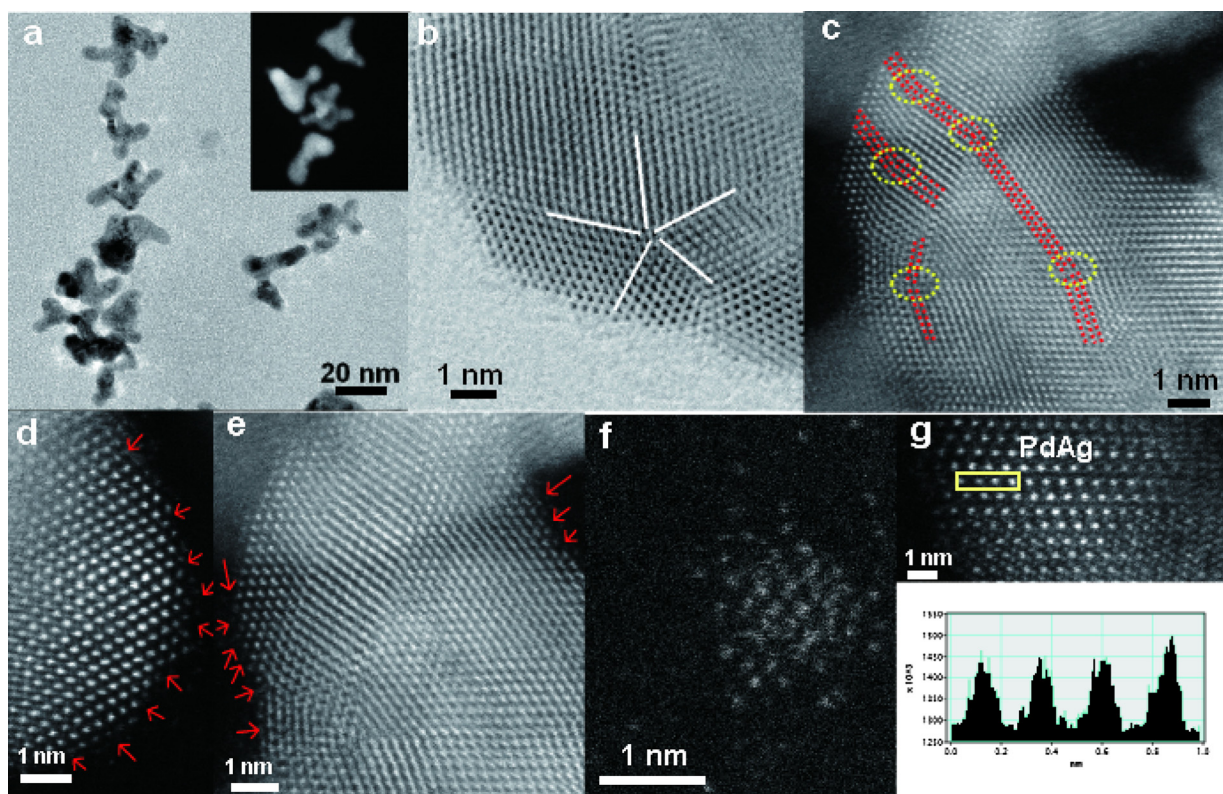
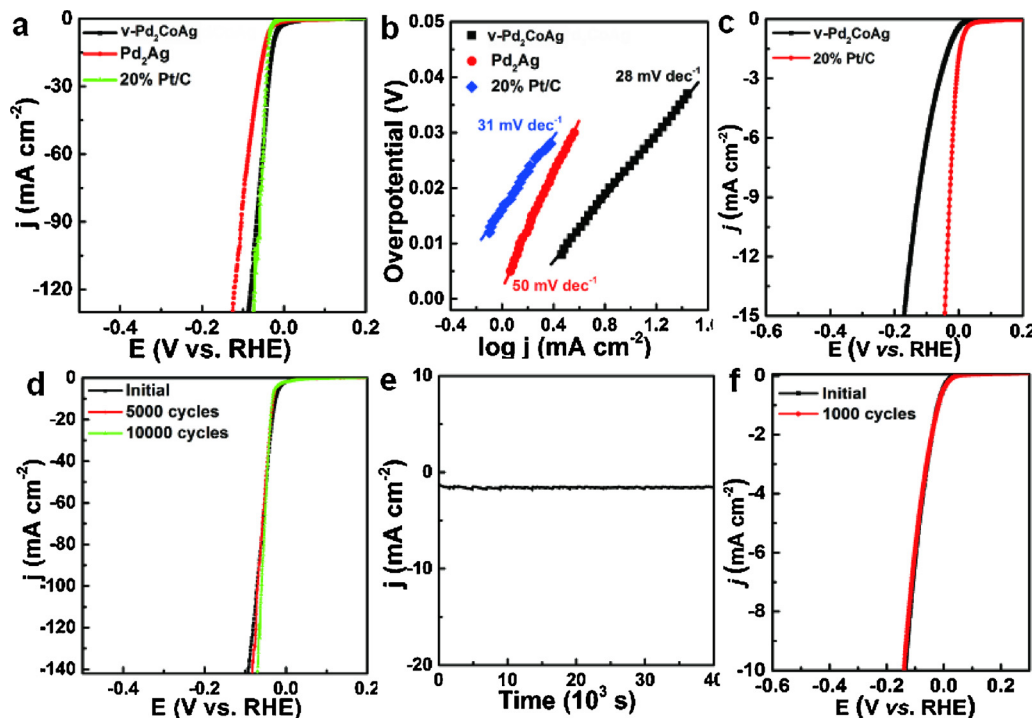


Fig. 2. (a) Representative TEM and (b) HRTEM images of the v-Pd₂CoAg. (c)–(e) Aberration-corrected HAADF-STEM images of the neighboring atom dispersion of v-Pd₂CoAg from different regions. (f) Magnified HAADF images of the v-Pd₂CoAg. (g) Line-scanning intensity profile obtained from the area highlighted with yellow rectangles in part g (For interpretation of the references to colour in this figure legend, the reader is referred to the web version of this article.).



scanning X-ray microprobe (PHI 5000 Versa, ULACPHI, Inc.) using Al K α radiation. The metal (Pd, Co, and Ag) loadings of the catalysts were determined by the inductively coupled plasma atomic emission spectroscopy (ThermoFisher, ICP-AES).

3. Results and discussion

3.1. Structural characterization of v-Pd₂CoAg NC

To create the abundant vacancies, Pd₂CoAg NCs capped by organic

Fig. 3. (a) HER polarization curves for the v-Pd₂CoAg NCs, Pd₂Ag NCs, and 20% Pt/C catalysts in 0.5 M H₂SO₄. (b) The corresponding Tafel plots. (c) HER polarization curves for the v-Pd₂CoAg NCs and 20% Pt/C catalysts in 1.0 M KOH. (d) Polarization curves before and after 10 000 CV cycles of the v-Pd₂CoAg NCs ranging from -0.18 to 0.20 V vs RHE in 0.5 M H₂SO₄. (e) Chronoamperometric technology at a constant overpotential of 20 mV of v-Pd₂CoAg NCs in 0.5 M H₂SO₄. (f) Polarization curves before and after 1000 CV cycles of the v-Pd₂CoAg NCs ranging from -0.18 to 0.20 V vs RHE in 1.0 M KOH.

Table 1

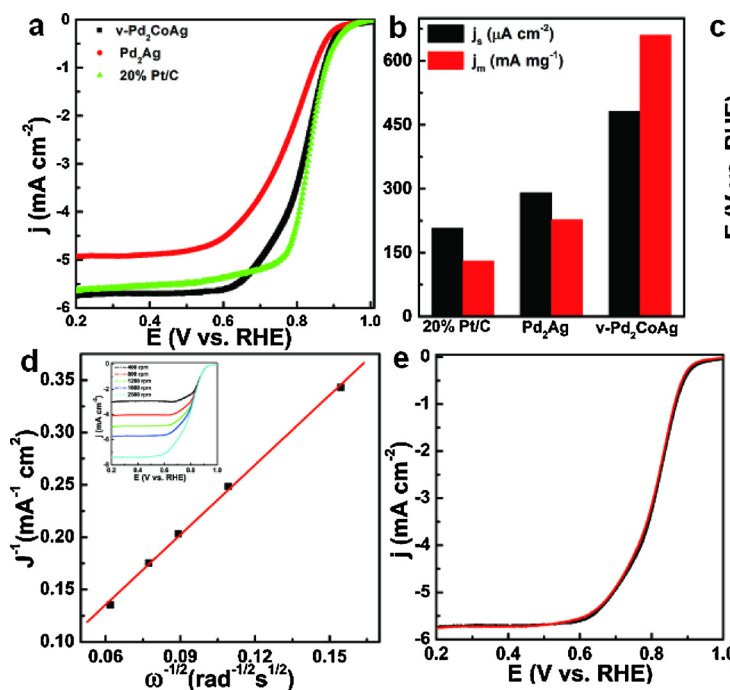
Comparison of the catalytic parameters of different HER catalysts.

Catalyst	Tafel slope [mV dec ⁻¹]	η_{10} [mV]	j_0 [mA cm ⁻²]
v-Pd ₂ CoAg NCs	28	24	1.38
Pd ₂ Ag NCs	50	52	0.89
20% Pt/C	31	45	0.64

amine were synthesized by a simple, one-pot, solid-liquid phase approach. Its metal content was controlled by the molar ratios of metal precursors, and the composition of the final products was determined by ICP-AES which was further supported by EDS (Fig. S1). These analyses demonstrate that the quantitative atomic ratio of Pd, Co and Ag in the corresponding v-Pd₂CoAg NCs is uniform and close to 55:24:21. Moreover, the XRD pattern (Fig. 1a) shows that the as-synthesized product owns a typical fcc structure. However, there are no typical diffraction peaks of Co or its oxides [17–19]. Meanwhile, the corresponding magnetization-magnetic field ((M – H)) plot of the v-Pd₂CoAg at 300 K is shown in Fig. 1b. Under a very small external magnetic field, it rapidly reaches magnetic saturation, confirming that the Co in twinned Pd₂CoAg NCs mainly exists in the alloy form.

Furthermore, XPS was applied to characterize the chemical state and electronic structure of the typical sample [12]. For the Pd and Ag segments, The Pd 3d and Ag 3d peaks can be well identified to metal (0) [17,18], as is shown in Fig. 1c and d. The peaks at 795.3 and 778.8 eV are assigned to Co 2p_{1/2} and Co2p_{3/2}, of the Co species (0) in v-Pd₂CoAg NCs, respectively. (Fig. 1e) [18]. The peaks at 802.3 and 783.2 eV are assigned to Co 2p_{1/2} and Co 2p_{3/2} of the CoO_x, respectively, arising from the surface oxidation of v-Pd₂CoAg. The binding energies of 532.7 eV and 531.6 eV are ascribed to the O vacancies (about 39.6%) and bridging oxo-groups (Co-O-Co), respectively (Fig. 1f). [25]. These XPS results confirm that the decorated CoO_x layer leads to charge redistribution on the interface of Pd₂CoAg NCs and CoO_x atomic vacancies, beneficial for promoting key electrocatalytic reactions [18,21,25]. It is worth mentioning that this novel one-pot synthesis method of v-Pd₂CoAg NCs has been extended to prepare v-Pd₂FeAg nanostructures (Fig. S2).

The TEM and STEM images show that the product possesses



multipod structures (Fig. 2a and inset of Fig. 2a), and the average diameter of the pod is approximately 5 nm A closer look at the pod ends (Fig. 2b) reveals the presence of a five-fold twinned structure, as marked by the white dotted lines. Meanwhile, as shown in Fig. 2c, a side view of the five-fold twinned multipod is also provided. [24] The lattice fringes are continuous through the entire multipod, and the twin planes or stacking faults are clearly observed across the edge-pod junction (Figs. 2c and S3) which may provide more catalytically active sites to enhance their catalytic activity. [20,24] Furthermore, we can observe that abundant vacancies are randomly scattered over the five-fold twinned surface and interface edge [17]. The corresponding high-angle annular dark-field (HAADF) aberration-corrected scanning transmission electron microscopy (Cs-STEM) images in Figs. 2d and e reveal that the defective regions (pointed out by the red arrow) mainly exist on the surface and the interface edge of the v-Pd₂CoAg NCs. Furthermore, the highly dispersed locations of brighter spots on the darker matrix reveal the abundant neighboring and the high density of atomically dispersed PdAg in the v-Pd₂CoAg NCs, further confirming the existence of abundant vacancies in the multipod (Fig. 2f). [20,24] From the intensity line profiles, PdAg atoms are neighbored by 0.23 nm in distance (Fig. 2g), corresponding to the (111) plane of PdAg.

3.2. HER activity and stability of catalysts

The electrocatalytic HER properties of as-obtained v-Pd₂CoAg NCs were measured and compared with that of Pd₂Ag NCs and 20% Pt/C (20 wt% loading) (Fig. S4). To perform such tests, the as-prepared samples were first deposited on the Graphene (G) via sonication (the mass ratio of NCs to G is 1/2) in hexane (Fig. S5) [24,26]. From polarization curves, it exhibits a small onset potential (Fig. 3a) of 0 mV vs RHE, which is more positive than that of Pd₂Ag and nearly same to Pt/C catalysts in 0.5 H₂SO₄. Furthermore, based on the log j ~ η plots (Fig. 3b, Tables 1 and S1), the v-Pd₂CoAg has a small Tafel slope of 28 mV dec⁻¹, suggesting that the HER on this catalyst is dominated by the Volmer-Tafel reaction mechanism [11,13,20,27]. The fast HER kinetics also enables it to reach a high current density of 10 mA cm⁻² at η as low as 24 mV, outperforming Pd₂Ag NCs (52 mV), Pt/C (45 mV) and most of the reported HER catalysts (Tables 1 and S1). Remarkably, its exchange current density (j_0) (1.38 mA cm⁻²) is higher than that of

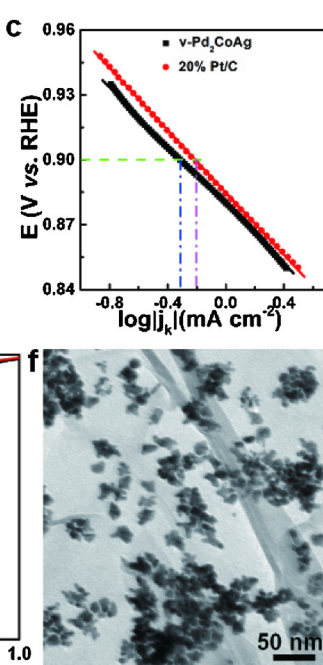


Fig. 4. (a) Polarization curves of v-Pd₂CoAg NCs, Pd₂Ag NCs, and 20% Pt/C for ORR in O₂-saturated 0.1 M KOH solution at a sweep rate of 10 mV s⁻¹. (b) Specific activity and mass activity of the v-Pd₂CoAg NCs, Pd₂Ag NCs, and 20% Pt/C at 0.90 V vs RHE. (c) The corresponding Tafel plots. (d) Inset: linear sweep voltammetry of v-Pd₂CoAg NCs in O₂ saturated 0.1 M KOH with a sweep rate of 5 mV s⁻¹ at the different rotation rates. Koutecky-Levich plot of v-Pd₂CoAg NCs at 0.40 V vs RHE. (e) v-Pd₂CoAg NCs before and after 5000 potential sweeps between 0.17 and 1.07 V vs RHE, respectively. (f) TEM of v-Pd₂CoAg NCs catalyst after the durability test.

Pd₂Ag (0.89 mA cm⁻²) and Pt/C (0.64 mA cm⁻²) catalysts (Table 1). Furthermore, Fig. 3c shows the HER performance of v-Pd₂CoAg in a 1.0 M aqueous KOH solution. It has a lower onset potential of -0.005 mV than Pd₂Ag, which is close to Pt/C. In addition, after 10,000 cycles or 40 000 s in 0.5 M H₂SO₄ v-Pd₂CoAg catalyst remains at a constant without obvious decline, implying the excellent cycling stability (Fig. 3d). Moreover, it also shows excellent stability in an alkaline solution, as shown in Fig. 3f.

3.3. ORR activity and stability of catalysts

The electrocatalytic activity of v-Pd₂CoAg NCs for ORR was evaluated in an O₂-saturated 0.1 M KOH solution using the RDE method [9,14,28]. As references, commercial Pt/C and Pd₂Ag NCs catalysts were also prepared and evaluated under the same conditions, as shown in Figs. 4a and S6. Both v-Pd₂CoAg and Pt/C require an onset potential of around 0.95 V to trigger the ORR. Meanwhile, to obtain more insight into the comparatively superior catalytic activity of those catalysts, their specific activity (J_s) and mass activity (J_m) values were calculated according to the method described elsewhere [28,29] and shown in Fig. 4b. J_s and J_m calculations were. In detail, the J_m and J_s are depicted as I₀ normalized to noble metal mass loading and corresponding to electrochemical active surface area (ECSA) (Figs. S7 and 4 c), respectively [29]. In 0.1 M KOH solution, the J_m of v-Pd₂CoAg is 5 times higher than that of Pt/C at 0.9 V, indicating the superior intrinsic catalytic activity of the former (Fig. 4b). The excellent ORR activity of the v-Pd₂CoAg is also apparent from the superior Tafel slope (66 mV dec⁻¹) at a low overpotential (Fig. 4c), close to that of the Pt/C (69 mV dec⁻¹) in 0.1 M KOH. On the other hand, the v-Pd₂CoAg catalyzes a 4-electron reduction to produce OH⁻ according to the Koutecky-Levich plots in Fig. 4d [30]. Additionally, it maintains even after 5000 cycles (Figs. 4e and S7b) with the almost unchanged morphology (Fig. 4f).

Based on the above results and in conjunction with recent theoretical calculations of Pd-based NCs [18,24,28–30], the remarkable bi-functional properties of v-Pd₂CoAg NCs can be ascribed to the presence of abundant vacancies and metal alloy interfaces on the junction area with increased steps, edges and kink sites, leading to a reduced coordination number of surface atoms [31,32]. Furthermore, the addition of Co not only increases the atomic vacancies of Pd₂Ag twinned interfaces, but also leads to the formation of oxygen vacancies on the surface of CoO_x [33,34]. The synergistic effect of the surface atomic vacancies and metal twinned interfaces of v-Pd₂CoAg NCs can tune the charge-density distribution on the surface of electrocatalysts, resulting in a change in the adsorption energy of atomic hydrogen or oxygen, and subsequently triggering the total increase in HER and ORR activities (Figs. 1 and 2).

4. Conclusion

In summary, we report a twinned Pd₂CoAg nanocrystal electrocatalyst with atomic vacancies and excellent HER and ORR activities close to that of commercial Pt/C. In detail, it exhibits high HER performance in acidic media with smaller overpotentials at 10 mA cm⁻² (24 mV) and lower Tafel slopes (28 mV dec⁻¹) as well as long term stability, which surpass the state-of-art Pt/C. While for ORR, it also reveals a superior onset reduction potential of 0.95 V (vs. RHE), a large mass activity of 0.660 A mg⁻¹_{Pd}, and superior long-term stability. As a result, the novel catalyst possesses excellent enhanced bifunctionality toward both ORR and HER, which can be attributed to the increased basic active sites of the atomic vacancies together with the twinned Pd₂CoAg interfaces. Such excellent ORR and HER activities of v-Pd₂CoAg NCs with strong stability and low noble metal loadings make them a promising electrocatalyst for fuel cells, water splitting or other electrochemical devices.

Author contributions

C. Y. Cheng, S. L. Liu designed the experiment. X. Q. Mu prepared the samples and tested the electrochemical performances. H. Zhang conducted the physicochemical characterizations. All authors contributed to the discussion and provided feedback on the manuscript.

Acknowledgements

This work was supported by the NSFC (21501096) and Natural Science Foundation of Jiangsu (BK20150086), China Postdoctoral Science Foundation funded project (2015M570466) and Foundation of the Jiangsu Education Committee (15KJB150020).

Appendix A. Supplementary data

Supplementary material related to this article can be found, in the online version, at doi:<https://doi.org/10.1016/j.apcatb.2018.09.067>.

References

- [1] S. Wang, S.P. Jiang, Prospects of fuel cell technologies, *Sci. Rev.* 4 (2017) 163–166.
- [2] B.C. Filiz, A.K. Figen, S. Pişkin, The remarkable role of metal promoters on the catalytic activity of Co-Cu based nanoparticles for boosting hydrogen evolution: ammonia borane hydrolysis, *Appl. Catal. B Environ.* 238 (2018) 365–380.
- [3] L.J. Yang, J.Y. Yu, Z.Q. Wei, G.X. Li, L.D. Cao, W.J. Zhou, S.W. Chen, Co-N-doped MoO₂ nanowires as efficient electrocatalysts for the oxygen reduction reaction and hydrogen evolution reaction, *Nano Energy* 41 (2017) 772–779.
- [4] V. Vij, S. Sultan, A.M. Harzandi, A. Meena, J.N. Tiwari, W.G. Lee, T. Yoon, K.S. Kim, Nickel-based electrocatalysts for energy-related applications: oxygen reduction, oxygen evolution, and hydrogen evolution reactions, *ACS Catal.* 7 (2017) 7196–7225.
- [5] S.C. Cai, Z.H. Meng, H.L. Tang, Y. Wang, P. Tsikararas, 3D Co-N-doped hollow carbon spheres as excellent bifunctional electrocatalysts for oxygen reduction reaction and oxygen evolution reaction, *Appl. Catal. B Environ.* 217 (2017) 477–484.
- [6] J. Ying, G.P. Jiang, Z.P. Cano, Z. Ma, Z.W. Chen, Spontaneous Weaving: 3D porous PtCu networks with ultrathin jagged nanowires for highly efficient oxygen reduction reaction, *Appl. Catal. B Environ.* 236 (2018) 359–367.
- [7] W.Q. Li, Y.L. Xiong, Z. Wang, M.J. Bao, J. Liu, D.P. He, S.C. Mu, Seed-mediated synthesis of large-diameter ternary TePtCo nanotubes for enhanced oxygen reduction reaction, *Appl. Catal. B Environ.* 231 (2018) 277–282.
- [8] Y.G. Zhao, Y.J. Wu, J.J. Liu, F. Wang, Dependent relationship between quantitative lattice contraction and enhanced oxygen reduction activity over Pt-Cu alloy catalysts, *ACS Appl. Mater. Interfaces* 9 (2017) 35740–35748.
- [9] H. Lv, X. Chen, D.D. Xu, Y.C. Hu, H.Q. Zheng, S.L. Suib, B. Liu, Ultrathin PdPt bimetallic nanowires with enhanced electrocatalytic performance for hydrogen evolution reaction, *Appl. Catal. B Environ.* 238 (2018) 525–532.
- [10] D. Gao, J.N. Guo, X. Cui, L. Yang, Y. Yang, H.C. He, P. Xiao, Y.H. Zhang, Three-dimensional dendritic structures of NiCoMo as efficient electrocatalysts for the hydrogen evolution reaction, *ACS Appl. Mater. Interfaces* 9 (2017) 22420–22431.
- [11] H.C. Yang, Y.J. Zhang, F. Hu, Q.B. Wang, Urchin-like CoP nanocrystals as hydrogen evolution reaction and oxygen reduction reaction dual-electrocatalyst with superior stability, *Nano Lett.* 15 (2015) 7616–7620.
- [12] M.X. Li, X.X. Liu, X.L. Hu, Fabrication of core-sheath NiCoP@FeP_x nanoarrays for efficient electrocatalytic hydrogen evolution, *ACS Sustainable Chem. Eng.* 6 (2018) 8847–8855.
- [13] M. Monai, T. Montini, E. Fonda, M. Crosara, J.J.D. Jaen, G. Adami, P. Fornasiero, Nanostructured PdPt nanoparticles: evidences of structure/performance relations in catalytic H₂ production reactions, *Appl. Catal. B Environ.* 236 (2018) 88–98.
- [14] W.P. Xiao, M.A.L. Cordeiro, M.X. Gong, L.L. Han, J. Wang, C. Bian, J. Zhu, H.L. Xin, D.L. Wang, Optimizing the ORR activity of Pd based nanocatalysts by tuning their strain and particle size, *J. Mater. Chem. A* 5 (2017) 9867–9872.
- [15] S. Ghosh, R.N. Basu, Multifunctional nanostructured electrocatalysts for energy conversion and storage: current status and perspectives, *Nanoscale* 10 (2018) 11241–11280.
- [16] Z. Zong, K.B. Xu, D.L. Li, Z.H. Tang, W. He, Z. Liu, X.F. Wang, Y. Tian, Peptide templated Au@Pd core-shell structures as efficient bi-functional electrocatalysts for both oxygen reduction and hydrogen evolution reactions, *J. Catal.* 361 (2018) 168–176.
- [17] Y.P. Zuo, D.W. Rao, S. Li, T.T. Li, G.L. Zhu, S.M. Chen, L. Song, Y. Chai, H. Han, Atomic vacancies control of Pd-based catalysts for enhanced electrochemical performance, *Adv. Mater.* 30 (2017) 1704171.
- [18] H.W. Wang, W.J. Luo, L.J. Zhu, Z.P. Zhao, B.E. Wz. Tu, X.X. Ke, M.L. Sui, C.F. Chen, Q. Chen, Y.J. Li, Y. Huang, PdCo alloy nanonetworts-polyallylamine inorganic-organic nanohybrids toward the oxygen reduction reaction, *Adv. Funct. Mater.* 28 (2018) 1707219.
- [19] C.L. Wang, S. Liu, D.D. Wang, Q.W. Chen, Interface Engineering of Ru-Co₃O₄ nanocomposites for enhancing CO oxidation, *J. Mater. Chem. A* 6 (2018) 11037–11043.

- [20] Y. Liu, S.L. Liu, Y. Wang, Q.H. Zhang, L. Gu, S.C. Zhao, D.D. Xu, Y.F. Li, J.C. Bao, Z.H. Dai, Ru Modulation effects in the synthesis of unique rod-Like Ni@Ni₂P-Ru heterostructures and their remarkable electrocatalytic hydrogen evolution performance, *J. Am. Chem. Soc.* 140 (2018) 2731–2734.
- [21] E. Fabbri, M. Nachtegaal, T. Binninger, X. Cheng, B.J. Kim, J. Durst, F. Bozza, T. Graule, R. Schäublin, L. Wiles, M. Pertoso, N.D. Danilovic, K.E. Ayers, T.J. Schmidt, Dynamic surface self-reconstruction is the key of highly active perovskite nano-electrocatalysts for water splitting, *Nat. Mater.* 16 (2017) 925–931.
- [22] B.K. Kim, S.K. Kim, S.K. Cho, J.J. Kim, Enhanced catalytic activity of electrodeposited Ni-Cu-P toward oxygen evolution reaction, *Appl. Catal. B Environ.* 237 (2018) 409–415.
- [23] C.Y. Wang, X.H. Sang, J.T.L. Gamler, D.P. Chen, R.R. Unocic, S.E. Skrabalak, Facet-dependent deposition of highly strained alloyed shells on intermetallic nanoparticles for enhanced electrocatalysis, *Nano Lett.* 17 (2017) 5526–5532.
- [24] S.L. Liu, Q.H. Zhang, Y.F. Li, M. Han, L. Gu, C.W. Nan, J.C. Bao, Five-fold twinned Pd₂NiAg nanocrystals with increased surface Ni site availability to improve oxygen reduction activity, *J. Am. Chem. Soc.* 137 (2015) 2820–2823.
- [25] Y.P. Bi, B.B. Zhang, L. Wang, Y.J. Zhang, Y. Ding, Ultrathin FeOOH nanolayers with rich oxygen vacancies on BiVO₄ photoanodes for efficient water oxidation, *Angew. Chem. Int. Ed.* 57 (2018) 2248.
- [26] Q. Li, S.H. Sun, Recent advances in the organic solution phase synthesis of metal nanoparticles and their electrocatalysis for energy conversion reactions, *Nano Energy* 29 (2016) 178–197.
- [27] J.X. Feng, S.Y. Tong, Y.X. Tong, G.R. Li, Pt-like hydrogen evolution electrocatalysis on PANI/CoP hybrid nanowires by weakening the shackles of hydrogen ions on the surfaces of catalysts, *J. Am. Chem. Soc.* 140 (2018) 5118–5126.
- [28] H.Y. Zhu, S. Zhang, D. Su, G.M. Jiang, S.H. Sun, Surface profile control of FeNiPt/Pt core/shell nanowires for oxygen reduction reaction, *Small* 11 (2015) 3545–3549.
- [29] Y. Liu, S.L. Liu, Z.W. Che, S.C. Zhao, X.X. Sheng, M. Han, J.C. Bao, Concave octahedral Pd@PdPt electrocatalysts integrating core-shell, alloy and concave structures for high-efficiency oxygen reduction and hydrogen evolution reactions, *J. Mater. Chem. A* 4 (2016) 16690–16697.
- [30] J. Liu, C.Q. Sun, W.G. Zhu, Origin of efficient oxygen reduction reaction on Pd monolayer supported on Pd-M (M = Ni, Fe) intermetallic alloy, *Electrochim. Acta* 282 (2018) 680–686.
- [31] H.J. Xu, J. Cao, C.F. Shan, B.K. Wang, P.X. Xi, W.S. Liu, Y. Tang, MOF-derived hollow CoS decorated with CeO_x nanoparticles for boosting oxygen evolution reaction electrocatalysis, *Angew. Chem. Int. Ed.* 57 (2018) 8654–8658.
- [32] Y. Pan, K.A. Sun, S.J. Liu, X. Cao, K.L. Wu, W.C. Cheong, Z. Chen, Y. Wang, Y. Li, Y.Q. Liu, D.S. Wang, Q. Peng, C. Chen, Y.D. Li, Core-shell ZIF-8@ZIF-67-derived CoP nanoparticle-embedded N-doped carbon nanotube hollow polyhedron for efficient overall water splitting, *J. Am. Chem. Soc.* 140 (2018) 2610–2618.
- [33] B. Ni, P. He, W.X. Liao, S.M. Chen, L. Gu, Y. Gong, K. Wang, J. Zhuang, L. Song, G. Zhou, X. Wang, Surface oxidation of AuNi heterodimers to achieve high activities toward hydrogen/oxygen evolution and oxygen reduction reactions, *Small* 14 (2018) 1703749.
- [34] G. Wan, C. Yang, W.P. Zhao, Q.R. Li, N. Wang, T. Li, H. Zhou, H.R. Chen, J.L. Shi, Anion-regulated selective generation of cobalt sites in carbon: toward superior bi-functional electrocatalysis, *Adv. Mater.* 29 (2017) 1703436.